Hindawi
International Transactions on Electrical Energy Systems
Volume 2022, Article ID 6082642, 14 pages
https://doi.org/10.1155/2022/6082642

Research Article

Day-Ahead Economic Dispatch of Renewable Energy System considering Wind and Photovoltaic Predicted Output

Xinghua Liu,[1] **Xiang Li**,[1] **Jiaqiang Tian**,[1] **Yubo Wang**,[1] **Gaoxi Xiao**,[2] **and Peng Wang**[2]

[1]*School of Electrical Engineering, Xi'an University of Technology, Xi'an 710048, China*
[2]*School of Electrical and Electronic Engineering, Nanyang Technological University, Singapore 639798, Singapore*

Correspondence should be addressed to Jiaqiang Tian; tianjiaqiang@xaut.edu.cn

Received 21 March 2022; Revised 28 April 2022; Accepted 4 May 2022; Published 1 June 2022

Academic Editor: B Rajanarayan Prusty

To alleviate the issues of global warming and energy crisis, countries are vigorously developing renewable energy technology. The integration of large-scale renewable energy, including wind energy, hydropower, and photovoltaic (PV), has a great impact on system operation scheduling and economic dispatch. This paper presents an economic dispatching method of wind-PV-CSP-hydro-battery system with wind and photovoltaic power generation as the main energy sources. The long short-term memory (LSTM) neural network is applied to predict wind and PV power, besides, the Latin Hypercube Sampling (LHS) method and the synchronous reduction algorithm are used to obtain 10 typical wind and PV power scenarios. A day-ahead economic dispatch model of wind-PV-CSP-hydro-battery mathematical model is established, and relevant constraints are considered. Concentrated solar power (CSP), hydropower stations, batteries, and transferable loads are used as flexible resources to increase the penetration rate of wind and photovoltaic power generation. Finally, three cases are tested to demonstrate the feasibility of the proposed model. The results show that: (1) LSTM neural network can well predict the output power of wind and photovoltaic power generation with a small root mean square error (RMSE). (2) The introduction of transferable loads and CSP power station into the renewable energy power system can effectively reduce the fluctuation and curtailment rates of wind power and PV power generation.

1. Introduction

Climate warming has become an indisputable fact in the world. The Chinese government has promised to reach carbon peak and carbon neutralization in 2030 and 2060, respectively [1–3]. For the power industry, developing large-scale renewable energy and reducing the use of thermal power units are effective ways to reduce carbon emissions. The renewable energy power generation reached 22148 billion kWh in 2020, including 466.5 billion kWh for wind power and 260.5 billion kWh for photovoltaic power [4]. For large-scale renewable energy, the uncertainty and randomness of its output power limit its energy utilization, especially for the economic dispatching of renewable energy power systems [5].

To reduce the uncertainty of renewable energy in economic dispatch, scholars have conducted a lot of research on the power side and load side. On the power side, the intermittence of wind and photovoltaic power generation is considered in the renewable energy obligation model, which improves the penetration of wind and photovoltaic power generation [6]. The complementarity of wind and PV power generation is used to reduce its randomness [7]. In [8], the direct cost, under estimation penalty cost and over estimation penalty cost are applied to quantify the usage of wind power and photovoltaic power generation. To improve the accuracy of power generation calculation, illumination and wind speed are predicted in [9, 10]. In [11–13], wind power and PV power plants are jointly dispatched, and economic dispatch is carried out considering the objectives of the maximum wind-solar joint benefit. In summary, the utilization rate and output characteristics of wind power and photovoltaic power generation can directly describe the uncertainty of their behavior. On the load side, users can follow the wind and photovoltaic power generation adaptively according to the power consumption curve. The flexible loads are employed in the scheduling model to suppress the uncertainty brought by large-scale wind power grid connections [14]. To decrease the uncertainty in wind power generation and improve the

penetration rate of wind power generation, transferable loads on the demand side are investigated [15]. The interruptible load is regarded as a virtual unit to tackle the challenges of having large-scale wind power integration into the power system [16]. The demand-side response resources function is fully tapped by analyzing the difference of different loads' responses to electricity price for solving the random fluctuation of wind power in [17]. In general, the rational use of flexible loads can reduce the uncertainty of wind power and photovoltaic power generation.

A short-term PV power generation output prediction method based on particle swarm optimization-deep belief network (PSO-DBN) is proposed in [18], although the PSO algorithm can optimal the DBN network, the optimization results are inevitably affected by the setting of parameters. References [19, 20] use the back propagation neural networks to predict wind power. However, this method may cause overlearning and aggravate prediction errors due to the increase in the number of nodes in the hidden layer. Therefore, it is necessary to find a suitable method to predict the output of wind and PV power based on the wind and PV power characteristics. The long short-term memory (LSTM) neural network is a kind of recurrent neural network (RNN) model that can deal with time series forecasting problems [21]. It can predict the information for the next time by learning the data of the previous time. Meanwhile, the transferable load has the best flexibility and the better users' satisfaction with electricity consumption than reducible load [22]. It should be noted that the high penetration of wind power and PV in power system cannot be ignored. Concentrated solar energy (CSP) has an excellent performance in improving the penetration of renewable energy due to its thermal energy storage (TES) [23–25]. References [26–28] incorporate hydropower stations and batteries into wind power generation and PV power generation systems, which can maximize the system's ability to accept wind and PV power generation, as well as the economy and reliability of power system operation. In the economic dispatch of power system with renewable energy, there are still two problems: (1) the prediction method of renewable energy cannot effectively reflect the output characteristics of renewable energy; (2) to reduce the fluctuation of renewable energy, how to reasonably combine flexible resources.

To address these issues, this paper investigates a day-ahead economic dispatch model of the pure renewable energy power system. It takes wind power generation and photovoltaic power generation as the main power supply, and CSP power plant, hydropower station, battery, and transferable load as flexible resources. Meanwhile, LSTM neural network is used to predict the wind and PV power. Besides, the Latin Hypercube Sampling (LHS) method and the synchronous back reduction algorithm are applied to obtain 10 typical wind and PV power scenarios. Ultimately, the CPLEX is employed to get the optimal solutions for the proposed model. Moreover, three cases are used to prove the effectiveness of the model. Compared with the literature, this paper possesses the following contributions:

(1) A day-ahead economic dispatch model of wind-PV-CSP-hydro-battery is established. Compared with references [7–10] including thermal power generation, this paper is more meaningful to the economic scheduling of purely renewable energy systems in the future.

(2) The LSTM neural network is used to learn the output characteristics of wind energy and photovoltaic power generation, which can achieve a better prediction effect than the traditional neural network [19, 20].

(3) The simulation results show that compared with hydro-battery [9] and hydro-CSP-battery [7], hydro-CSP-battery-translatable load as flexible resources can better reduce the fluctuation of wind power and photovoltaic.

The rest of this paper is arranged as follows: In Section 2, a day-ahead economic dispatch model of wind-PV-CSP-hydro-battery is established. Section 3 shows the forecasting method of wind and PV output and introduces the solving steps of the day-ahead economic dispatch model of wind-PV-CSP-hydro-battery. The relevant cases are set up for proving the validity of the model, and the corresponding results are obtained by case simulation in Section 4. Finally, some concluding remarks are given in Section 5.

2. Model Formulation

To improve the flexibility of power system and reduce the fluctuation of renewable energy, this paper establishes a day-ahead economic dispatch model with the minimum sum of the economic costs of wind power, PV power generation, CSP power station, hydropower station, storage battery, and transferable load. In the meantime, the relevant constraints for each power generation unit also are considered, as shown in Figure 1.

2.1. Objective Function. In our work, the cost objective function includes wind power generation cost, PV power generation cost, CSP power station operation cost, CSP power station spinning reservation cost, hydropower generation cost, battery cost, and transferable load cost. The mathematical expression of economic cost objective function is given as follows:

$$\min C = C_w + C_{pv} + C_{csp} + C_h + C_b + C_{tl}, \tag{1}$$

where C is the total cost, C_w is wind power generation cost, C_{pv} is PV power generation cost, C_{csp} is CSP power station cost, C_h is hydropower generation cost, C_b is the battery cost, and C_{tl} is the compensation cost of the transferable load.

The cost of wind power generation and PV power generation is shown as follows:

$$C_w = \sum_{t=1}^{T} \sum_{j=1}^{N_w} K_{W,j} P_{j,t}, \tag{2}$$

$$C_{pv} = \sum_{t=1}^{T} \sum_{k=1}^{N_{pv}} K_{PV,k} P_{k,t}, \tag{3}$$

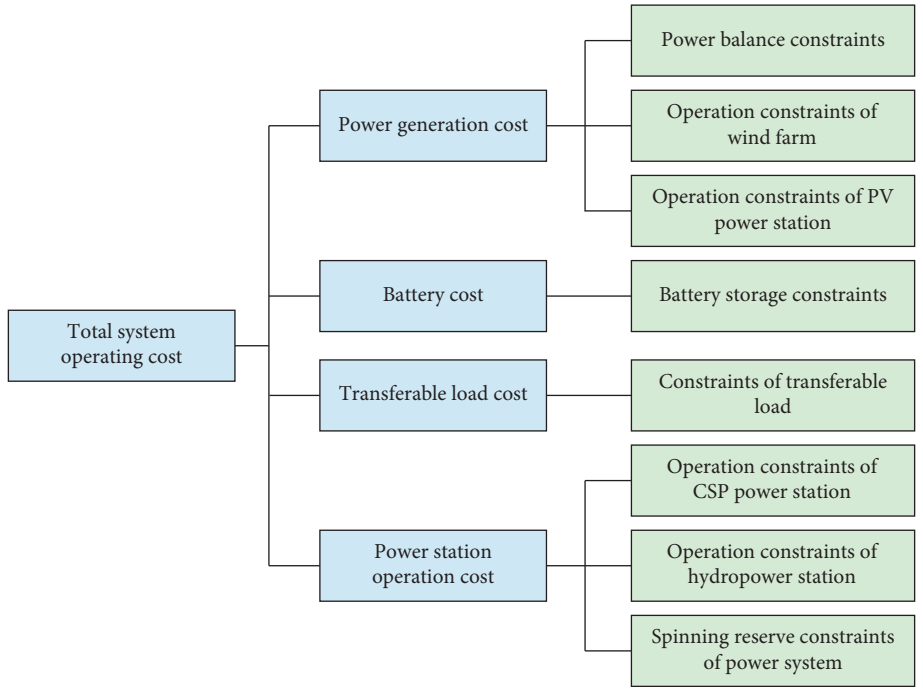

Figure 1: System operating costs and constraints.

where j is wind farms index, N_w is the total number of wind farm, $K_{W,j}$ is the cost coefficient of the j-th wind farm, $P_{j,t}$ is the output power of the j-th wind farm at time t. k is PV power station index, N_{pv} is the total number of PV power station, $K_{PV,k}$ is the cost coefficient of the k-th PV power station, and $P_{k,t}$ is the output power of the k-th PV power station at time t.

The cost of CSP power station has two parts, the first part is the operation cost of CSP power station, and the second part is the spinning reverse cost, which is stated as follows:

$$C_{csp} = \sum_{t=1}^{T} \sum_{l=1}^{N_{csp}} \left(K_{CSP,l} P_{l,t} + K_{CSP,R,l} P_{l,t,r} \right), \tag{4}$$

where l is CSP power station index, N_{csp} is the total number of CSP power stations, $K_{CSP,l}$ is the operation cost of the l-th CSP power station, $P_{l,t}$ is the output power of the l-th CSP power station at time t, $K_{CSP,R,l}$ is the spinning reverse cost of the l-th CSP power station, and $P_{l,t,r}$ is the spinning reverse power of the l-th CSP power station at time t.

The cost of hydropower station and the cost of battery are as follows:

$$C_h = \sum_{t=1}^{T} \sum_{m=1}^{N_h} K_{H,m} P_{m,t}, \tag{5}$$

$$C_b = \sum_{t=1}^{T} \sum_{n=1}^{N_b} K_{B,n} P_{n,t}, \tag{6}$$

where m is the hydropower station index, N_h is the total number of hydropower stations, $K_{H,m}$ is the cost coefficient of the m-th hydropower station, $P_{m,t}$ is the output power of the m-th hydropower station at time t, n is the battery, N_b is the total number of batteries, $K_{B,n}$ is the cost coefficient of the n-th battery, and $P_{n,t}$ is the output power of the n-th battery at time t.

The compensation cost of the transferable load is given as follows:

$$C_{tl} = \sum_{t \in T_{tl}} \sum_{t_{tl}=t_{tl}^{s}}^{t_{tl}^{e}} \left(C_{tl,t} P_{t,tl} U_{tl} \right), \tag{7}$$

where T_{tl} is the original operation time set of transferable load, $[t_{tl}^{s}, t_{tl}^{e}]$ is the transferable period of load, t_{tl}^{s}, t_{tl}^{e} are the start time and the end time of transferable period, $C_{tl,t}$ is the compensation cost of transferable load at time t, $P_{t,tl}$ is the power transferred from time t to tl, U_{tl} is the status of the transferable load, $U_{tl} = 1$ means the load transferred to time tl and $U_{tl} = 0$ otherwise.

2.2. Constraint Condition

2.2.1. Power Balance Constraints. To maintain the power balance of the system, the power balance constraint is established as Eq. (8). It is defined as the sum of the output power of j-th wind farm, the output power of k-th PV power station, the output power of l-th CSP power station, the output power of the m-th hydropower station, and the output power of the n-th battery equals the load of power system considering the transferable load. The specific formulas are as follows:

$$\sum_{j=1}^{N_w} P_{j,t} + \sum_{k=1}^{N_{pv}} P_{k,t} + \sum_{l=1}^{N_{csp}} P_{l,t} + \sum_{m=1}^{N_h} P_{m,t} + \sum_{n=1}^{N_b} P_{n,t} = P_{L,t} \quad \forall t \in [1, T], \tag{8}$$

$$P_{L,t} = P_{L_0,t} + P_{tl}, \tag{9}$$

where $P_{L,t}$ is the load of power system considering the transferable load, $P_{L_0,t}$ is the load of power system not considering the transferable load, and P_{tl} is the load transferred to time t.

2.2.2. Operation Constraints of Wind Farm. Wind farm operation constraints include the upper and lower limits constraint of the output power of j-th wind farm and forecast power constraint. The specific formulas are as follows:

$$0 \le P_{j,t} \le P_j^{\max}, \quad \forall t \in [1,T], \forall j \in [1,N_w], \tag{10}$$

$$P_{j,t} = P_{j,t,f} + P_{j,t,e}, \quad \forall t \in [1,T], \forall j \in [1,N_w], \tag{11}$$

where $P_j^{\max}$ is the maximum power of the j-th wind farm, $P_{j,t,f}$, $P_{j,t,e}$ are the forecast power and forecast error power of the j-th wind farm at time t.

2.2.3. Operation Constraints of PV Power Station. PV power station operation constraints include the upper and lower limits constraint of the output power of k-th PV power station and forecast power constraint. The specific formulas are as follows:

$$0 \le P_{k,t} \le P_k^{\max}, \quad \forall t \in [1,T], \forall k \in [1,N_{pv}], \tag{12}$$

$$P_{k,t} = P_{k,t,f} + P_{k,t,e}, \quad \forall t \in [1,T], \forall k \in [1,N_{pv}], \tag{13}$$

where $P_k^{\max}$ is the maximum power of the k-th PV power station, and $P_{k,t,f}$, $P_{k,t,e}$ are the forecast power and forecast error power of the k-th PV power station at time t.

2.2.4. Operation Constraints of CSP Power Station. The CSP power station can provide a spinning reserve because it has thermal energy storage (TES) units. The constraints of a CSP power station include upper and lower limits of the output power, upper and lower limits of TES discharge and charging power, positive and negative spinning reserve constraints provided by TES of CSP power station, and capacity constraints of TES of CSP power station. The specific formulas are as follows [9]:

$$P_{l,t} = P_{l,t,d}^{TES} - P_{l,t,c}^{TES}, \ \forall t \in [1,T], \forall l \in [1,N_{CSP}], \tag{14}$$

$$0 \le P_{l,t,d}^{TES} + P_{l,t,r+}^{TES} \le P_{l,t,d}^{TES,\max} Y_{l,t}, \ \forall t \in [1,T], \forall l \in [1,N_{CSP}], \tag{15}$$

$$0 \le P_{l,t,c}^{TES} + P_{l,t,r-}^{TES} \le P_{l,t,c}^{TES,\max}\left(1 - Y_{l,t}\right), \ \forall t \in [1,T], \forall l \in [1,N_{CSP}], \tag{16}$$

$$0 \le P_{l,t,r+}^{TES} \le P_{l,t,d}^{TES,\max}, \ \forall t \in [1,T], \forall l \in [1,N_{CSP}], \tag{17}$$

$$0 \le P_{l,t,r-}^{TES} \le P_{l,t,c}^{TES,\max}, \ \forall t \in [1,T], \forall l \in [1,N_{CSP}], \tag{18}$$

$$P_{l,t,r} = P_{l,t,r+}^{TES} + P_{l,t,r-}^{TES}, \ \forall t \in [1,T], \forall l \in [1,N_{CSP}], \tag{19}$$

where $P_l^{\max}$ is the maximum power of the l-th CSP power station, $P_{l,t,d}^{TES}$, $P_{l,t,c}^{TES}$ are the TES discharge power and the TES charge power of the l-th CSP power station at time t, $P_{l,t,r+}^{TES}$, $P_{l,t,r-}^{TES}$ are the positive spinning reserve and the negative spinning reserve provided by TES of the l-th CSP power station at time t, $P_{l,t,d}^{TES}$, $P_{l,t,c}^{TES}$ are the TES maximum discharge power and the TES maximum charge power of the l-th CSP power station at time t, $Y_{l,t}$ is state variable, $Y_{l,t} = 1$ means TES is discharging, while $Y_{l,t} = 0$ means TES is charging.

2.2.5. Operation Constraints of Hydropower Station. The constraints of hydropower station include upper and lower limits of the output power of hydropower station, storage capacity, and discharge capacity constraints of hydropower station, neglecting the spillage of hydropower station, which is shown as follows:

$$\begin{aligned} P_{m,t} = {} & \rho_{1,m}\left(V_{m,t}\right)^2 + \rho_{2,m}\left(Q_{m,t}\right)^2 + \rho_{3,m} V_{m,t} Q_{m,t} \\ & + \rho_{4,m} V_{m,t} + \rho_{5,m} Q_{m,t} + \rho_{6,m}, \end{aligned} \tag{20}$$

$$P_m^{\min} \le P_{m,t} \le P_m^{\max}, \quad \forall t \in [1,T], \forall m \in [1,N_h], \tag{21}$$

$$V_m^{\min} \le V_{m,t} \le V_m^{\max}, \quad \forall t \in [1,T], \forall m \in [1,N_h], \tag{22}$$

$$Q_m^{\min} \le Q_{m,t} \le Q_m^{\max}, \quad \forall t \in [1,T], \forall m \in [1,N_h], \tag{23}$$

$$\begin{aligned} V_{m,t+1} = {} & V_{m,t} + I_{m,t} - Q_{m,t} + \sum_{o=1}^{N_{ul}} Q_{o,(t-\tau_{om})}, \\ & \forall t \in [1,T], \forall m \in [1,N_h], \end{aligned} \tag{24}$$

where $\rho_{1,m}, \rho_{2,m}, \rho_{3,m}, \rho_{4,m}, \rho_{5,m}, \rho_{6,m}$ are the hydropower generation coefficients, $P_m^{\max}$, $P_m^{\min}$ are the maximum output power and the minimum output power of the m-th hydropower station, $V_{m,t}$, $V_{m,t+1}$ are the storage capacity of the reservoir of the m-th hydropower station at time t and time $t+1$, $V_m^{\max}$, $V_m^{\min}$ are the maximum and the minimum storage capacity of the reservoir of the m-th hydropower station, $Q_{m,t}$ is the outflow of the m-th hydropower station at time t, $Q_m^{\max}$, $Q_m^{\min}$ are the maximum and the minimum outflow of the m-th hydropower station, $I_{m,t}$ is the inflow of the m-th hydropower station at time t, o is an upstream hydropower station of the m-th hydropower station, τ_{om} is the time delay from the o-th hydropower station to the m-th hydropower station, and $Q_{o,(t-\tau_{om})}$ is the outflow of the o-th hydropower station by time $t - \tau_{om}$.

2.2.6. Constraints of Battery. The constraints of battery include capacity constraints, charge and discharge power constraints, and charge and discharge state constraints. The specific formulas are as follows:

$$E_n^{\min} \le E_{n,t} \le E_n^{\max}, \quad \forall t \in [1,T], \forall n \in [1,N_b], \tag{25}$$

$$0 \le P_{n,t}^c \le P_n^{c,\max}, \quad \forall t \in [1,T], \forall n \in [1,N_b], \tag{26}$$

$$0 \le P_{n,t}^{d} \le P_{n}^{d,\max}, \quad \forall t \in [1,T], \forall n \in [1,N_b], \tag{27}$$

$$c_{n,t} + d_{n,t} \le 1, \quad \forall t \in [1,T], \forall n \in [1,N_b], \tag{28}$$

$$P_{n,t} = c_{n,t}P_{n,t}^{c} + d_{n,t}P_{n,t}^{d}, \quad \forall t \in [1,T], \forall n \in [1,N_b], \tag{29}$$

$$E_{n,t} = \frac{E_{n,t-1} + P_{n,t}^{c}\eta_n^{c}\Delta t_n - P_{n,t}^{d}\Delta t_n}{\eta_n^{d}}, \quad \forall n \in [1,N_b], \tag{30}$$

where $E_{n,t}$, $E_{n,(t-1)}$ are the capacities of the n-th battery at time t and time $t-1$, $E_n^{\max}$, $E_n^{\min}$ are the maximum and the minimum capacities of the n-th battery, $P_{n,t}^{c}$, $P_{n,t}^{d}$ are the charge and discharge power of the n-th battery at time t, $P_n^{c,\max}$, $P_n^{d,\max}$ are the maximum charge power and the maximum discharge power of the n-th battery, $c_{n,t}$, $d_{n,t}$ are the states of charge and discharge of the n-th battery at time t, $c_{n,t} = 0$, $c_{n,t} = 1$ means not charge and charge of the n-th battery at time t, $d_{n,t} = 0$, $d_{n,t} = 1$ means not discharge and discharge of the n-th battery at time t, η_n^{c}, η_n^{d} are the charge and the discharge efficiencies, respectively, and Δt_n is the unit time interval.

2.2.7. Spinning Reserve Constraints of Power System. Spinning reserve constraints of power system include up spinning reserve and down spinning reserve. The specific formulas are as follows:

$$\sum_{m=1}^{N_h}\left(P_m^{\max} - P_{m,t}\right) + \sum_{l=1}^{N_{csp}} P_{l,t,r+}^{TES} + \sum_{n=1}^{N_b}\left(P_n^{d,\max} - P_{n,t}^{d}\right) \ge RU_s, \quad \forall t \in [1,T], \tag{31}$$

$$\sum_{m=1}^{N_h}\left(P_{m,t} - P_m^{\min}\right) + \sum_{l=1}^{N_{csp}} P_{l,t,r-}^{TES} + \sum_{n=1}^{N_b}\left(P_n^{c,\max} - P_{n,t}^{c}\right) \ge RD_s, \quad \forall t \in [1,T], \tag{32}$$

where RU_{pv}, RD_s are the up spinning reserve and down spinning reserve of the power system.

2.2.8. Constraints of Transferable Load. Based on not affecting the user's satisfaction with power consumption, the transferable load shall be limited to a certain time area, that is, only the transferable load within the allowable time shall be considered. The specific formula is as follows:

(a) Transferable load within allowable time:

$$P_{tl} = U_{tl}P_{t,tl} + \left[1 - \sum_{t_{tl}=t_{tl}^{s}}^{t_{tl}^{e}} U_{tl}\right]P_{t,tl}, \quad \forall t \in T_{tl}, \forall t_{tl} \in [t_{tl}^{s}, t_{tl}^{e}], \tag{33}$$

where P_{tl} is transfer power of the transferable load.

(b) Transferable load in disallowed time:

$$P_{tl} = 0, \quad \forall t \notin T_{tl}, \forall t_{tl} \notin [t_{tl}^{s}, t_{tl}^{e}]. \tag{34}$$

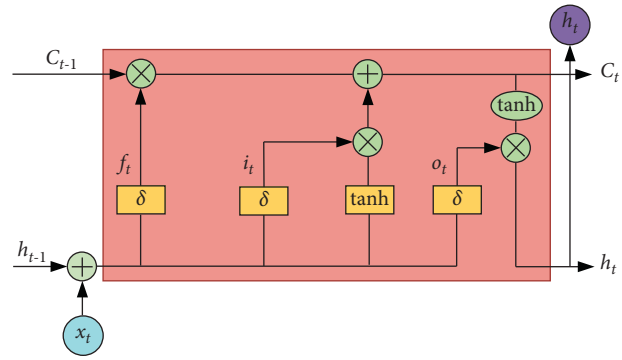

Figure 2: Structure diagram of LSTM neural network.

3. Solution Steps

3.1. Forecast Wind Power and PV Power. Wind power and PV power are uncertain and random. If the deterministic wind power and PV power data are used to solve the economic dispatch, it will influence the veracity of the economic dispatch results. Therefore, it is necessary to use historical data to predict wind power and PV power.

The LSTM neural network has a special gate structure, which solves the gradient vanishing problem in the RNN neural network [29]. It can predict the information of the next time by learning data of the previous time. Therefore, LSTM neural network is used to predict wind power and PV power. The specific structure of LSTM neural network is shown in Figure 2 [30].

In Figure 2, x_t is the input variable of the LSTM neural network at time t, h_{t-1}, h_t are the output variables of the LSTM neural network at time $t-1$ and t, C_{t-1}, C_t are the memory units status at time $t-1$ and t, f_t is forget gate, i_t is input gate, o_t is output gate, $\widetilde{C}_{t-1}$ is memory unit status, and δ is the sigmoid function. The mathematical formula of each gate is as follows [31]:

$$\begin{cases} f_t = \delta\left(W_{h,f} * h_{t-1} + W_{x,f} * x_t + b_f\right) \\ i_t = \delta\left(W_{h,i} * h_{t-1} + W_{x,i} * x_t + b_i\right) \\ \widetilde{C}_{t-1} = \tanh\left(W_{h,c} * h_{t-1} + W_{x,c} * x_t + b_c\right) \\ o_t = \delta\left(W_{h,o} * h_{t-1} + W_{x,o} * x_t + b_o\right) \\ C_t = f_t * C_{t-1} + i_t * \widetilde{C}_{t-1} \\ h_t = o_t * \tanh\left(C_t\right) \end{cases}, \tag{35}$$

where $W_{h,f}$ $W_{h,i}$ $W_{h,c}$, $W_{h,o}$ are the recursive weight matrixes of f_t, i_t, $\widetilde{C}_{t-1}$, o_t. $W_{x,f}$, $W_{x,i}$, $W_{x,c}$, $W_{x,o}$ are the input weight matrixes of f_t, i_t, $\widetilde{C}_{t-1}$, o_t, respectively, and b_f, b_i, b_c, b_o are the offset matrixes of f_t, i_t, $\widetilde{C}_{t-1}$, o_t, respectively [32].

The explanation of each gate in Figure 2 is as follows: the forget gate f_t determines the information to be retained and discarded through the sigmoid function, the input gate i_t determines the information to be updated through the sigmoid function. $\widetilde{C}_{t-1}$ is generated by the tanh function. The output gate o_t firstly obtains the initial output through the sigmoid function and then multiplies the initial output with

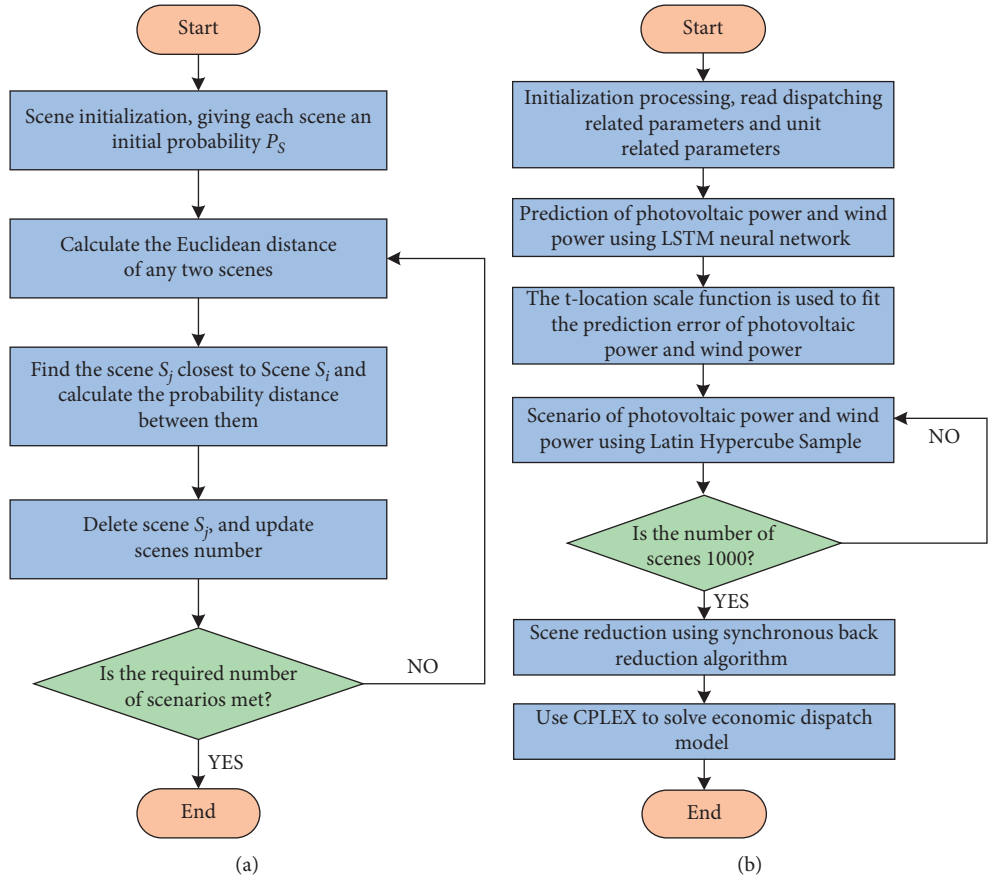

Figure 3: Flow chart: (a) Synchronous back reduction algorithm. (b) Solution steps of mathematical model.

C_t which through the tanh function layer at the time t to obtain the final output h_t.

3.2. Prediction Error Fitting of Wind Power and PV Power. Most literature regards the probability distribution of prediction error of wind power and PV power generation as having a normal distribution. However, according to references [33, 34], the t-Location Scale function may better reflect the probability distribution of prediction error of wind power and PV power generation.

$$f(\delta) = \frac{\Gamma\left(\left(v_t+1\right)/2\right)}{\sigma_t\sqrt{v_t\pi}\Gamma\left(v_t/2\right)}\left[\frac{v_t+\left(\left(\delta-\mu_t\right)/\sigma_t\right)^2}{v_t}\right]^{-\left(\left(v_t+1\right)/2\right)}, \tag{36}$$

where μ_t is the mean, σ_t is the variance, v_t $(v_t > 0)$ is the free degree.

3.3. Scenario Generation and Reduction of Wind Power and PV Power. LHS method has the characteristics of stratified sampling and disordered sorting [35], which avoids the disadvantages of clustering and repeated sampling. Therefore, the LHS method is adopted to generate 1000 wind power and PV power scenarios.

To simulate economic dispatch for 1000 scenarios could be highly time consuming. It is therefore necessary to reduce the number of scenarios. In this paper, the synchronous back reduction algorithm [36] is used to solve the problem. The solution flow chart is shown in Figure 3. The specific steps are given inTable 1.

4. Case Simulation

In this paper, the data of wind power and PV power generation are from Elia company in Belgium. The cost coefficients of wind power and PV power generation are adopted from reference [10], the relevant parameters of hydropower station are from reference [17], and the coefficient of CSP station comes from [35]. The relevant parameters of the storage battery are shown in Table 2. The system load data are shown in Table 3, and 5% of the system reserve is considered. The case simulation adopts a PV power station, a wind farm, two hydropower stations, two batteries and a CSP station, and three different cases as shown below are set to verify the mathematical model. Matlab R2019b is used to predict wind power and PV power generation, and the mathematic model is solved by CPLEX.

Case 1. Economic dispatch of wind-PV-hydro-battery.

Case 2. Economic dispatch of wind-PV-hydro-CSP-battery.

Table 1: The specific steps of synchronous back reduction algorithm.

Step 1: Assign probabilities to N scenarios generated by sample $P_s = 1/N$.
Step 2: Calculate the Euclidean distance between any two scenarios S_i and S_j $(S_i \neq S_j)$ in the scenario set: $DT_{i,j} = \left\|S_i - S_j\right\|$.
Step 3: The probability distance between scenario S_i and scenario S_m with the smallest Euclidean distance is calculated. The distance formula is as follows: $P_{DT_s} = \min\left\{DT_{i,m} \middle| S_i \neq S_m\right\} \times P_s$.
Step 4: Calculate the probability distance between two scenarios in the scenario set, then sort the scenario according to the probability distance: $P_{DT} = \min\left\{P_{DT_s} \middle| 1 \leq S \leq N\right\}$.
Step 5: Update the scenario probability $P_{DT} = \min\left\{P_{DT_s} \middle| 1 \leq S \leq N\right\}$, remove the scenario S_m from the original scenario set, change the number of scenarios to $N = N - 1$, and repeat Step 2 to Step 5 until the number of scenarios reaches the required number.

Table 2: Battery parameters.

Parameter	Battery charge and discharge efficiency	Battery charge and discharge power (MW)	Maximum battery capacity	Minimum battery capacity
Value	0.95	20	100 MW•h	35 MW•h

Table 3: Prediction values of system load.

Time/h	1	2	3	4	5	6
Power/MW	1740.8	1664.53	1720.35	1997.6	2122.38	2365.49
Time/h	7	8	9	10	11	12
Power/MW	2667.35	3061.15	3345.56	3665.04	3701.22	3703.08
Time/h	13	14	15	16	17	18
Power/MW	3587.42	3513.2	2577.89	2848.33	3224.32	3370.84
Time/h	19	20	21	22	23	24
Power/MW	3322.42	2855.17	2404.45	2351.39	2226.54	2097.86

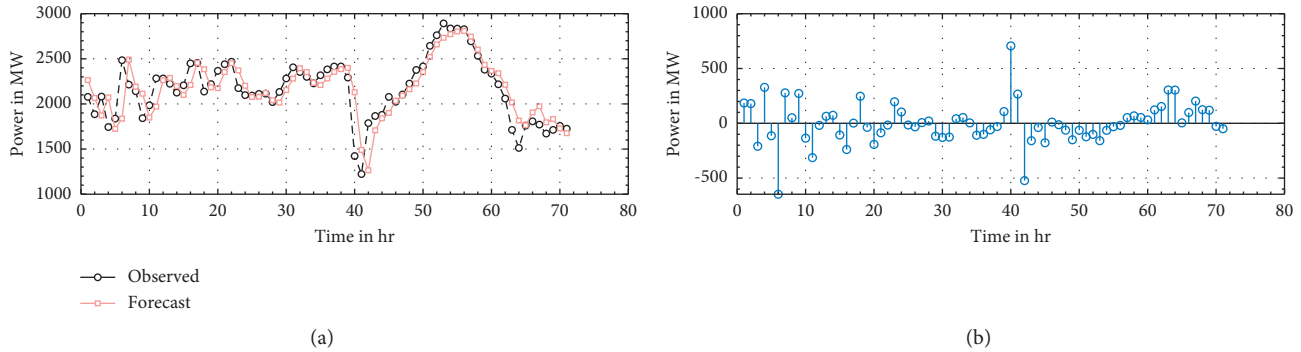

Figure 4: Forecast of wind power: (a) Wind power forecast curve. (b) Root mean square error of wind power forecast.

Case 3. Economic dispatch of wind-PV-hydro-CSP-battery considering transferable load.

4.1. Forecast of Wind Power and PV Power. The data of wind power and PV are from the measured data from July 1, 2020 to September 1, 2020 provided by Elia company in Belgium. The sampling time of wind power and PV is 1 hour. A total of 24 data sets are sampled a day, and the historical data of wind power and PV are 2208 points, respectively.

The LSTM neural network is used to predict wind power and PV. The hidden layer of LSTM neural network is taken 200 layers. The first 90% of the historical data sequence is used for training and the last 10% is used for testing. The solver is set to 'Adam'. According to the different output characteristics of PV and wind power, PV shall carry out 250 rounds of training. We specify the initial learning rate of 0.005 and reduce the learning rate by multiplying the factor of 0.2 after 125 rounds of training. We conducted 300 rounds of wind power training and specified an initial learning rate of 0.005. After 150 rounds of training, multiplying by a factor of 0.2 reduces the learning rate.

To enhance the diagnostic accuracy of wind power output, K-means clustering method is adopted for processing the historical data of wind power, and the historical data of wind power with similar output characteristics are used for prediction three days before the prediction date. The forecasted wind power output data is shown in Figure 4. The output characteristics of PV power generation are obvious, and the historical data are not processed. The forecasted PV

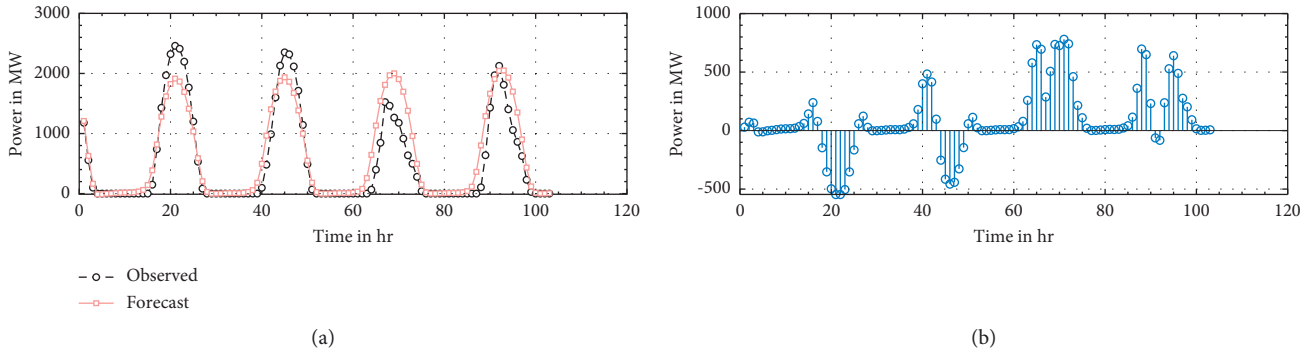

Figure 5: Forecast of PV: (a) PV forecast curve. (b) Root mean square error of PV forecast.

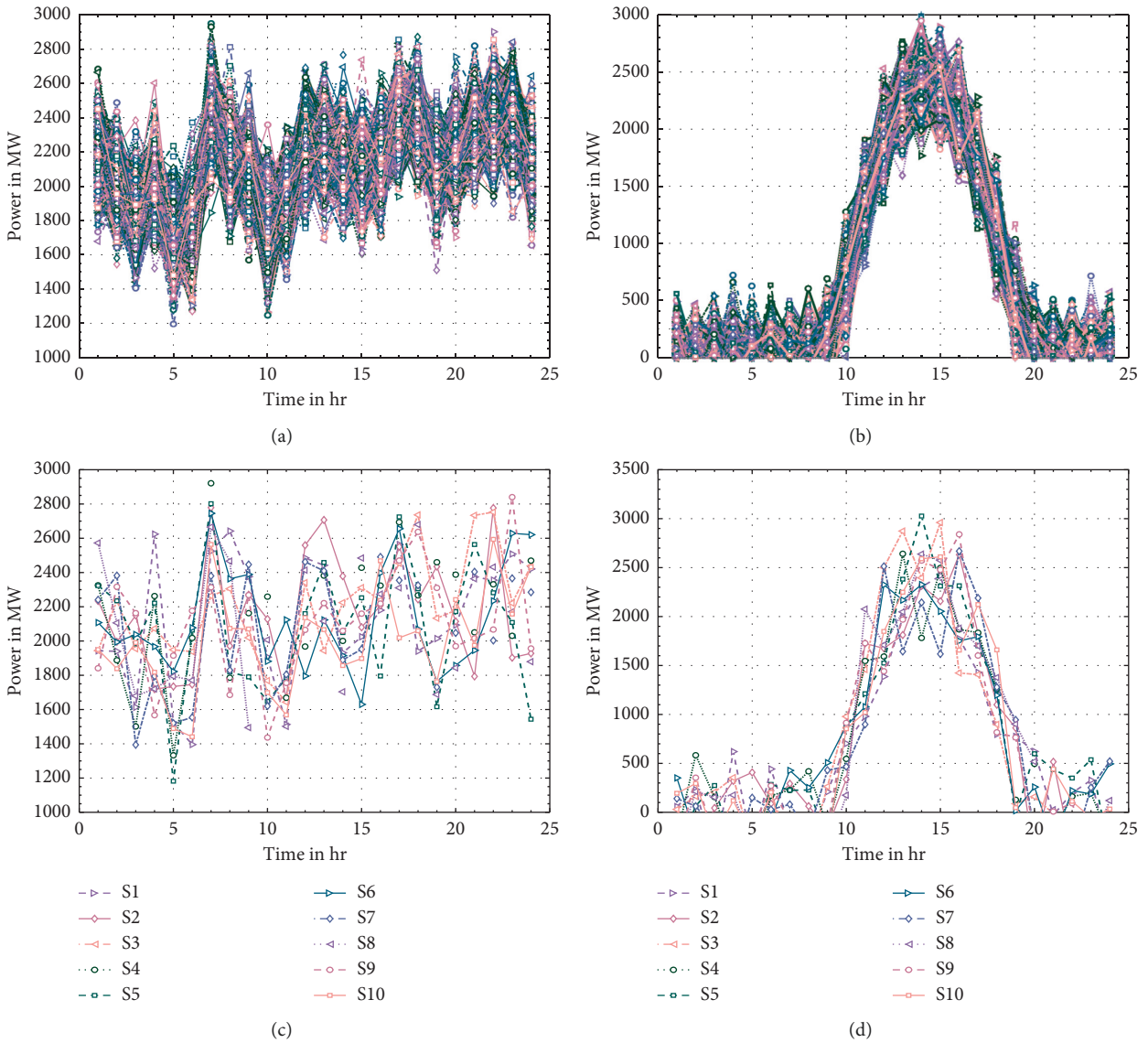

Figure 6: Wind and PV scenarios: (a) 1000 wind power scenarios. (b) 1000 PV scenarios. (c) 10 typical wind power scenarios. (d) 10 typical PV scenarios.

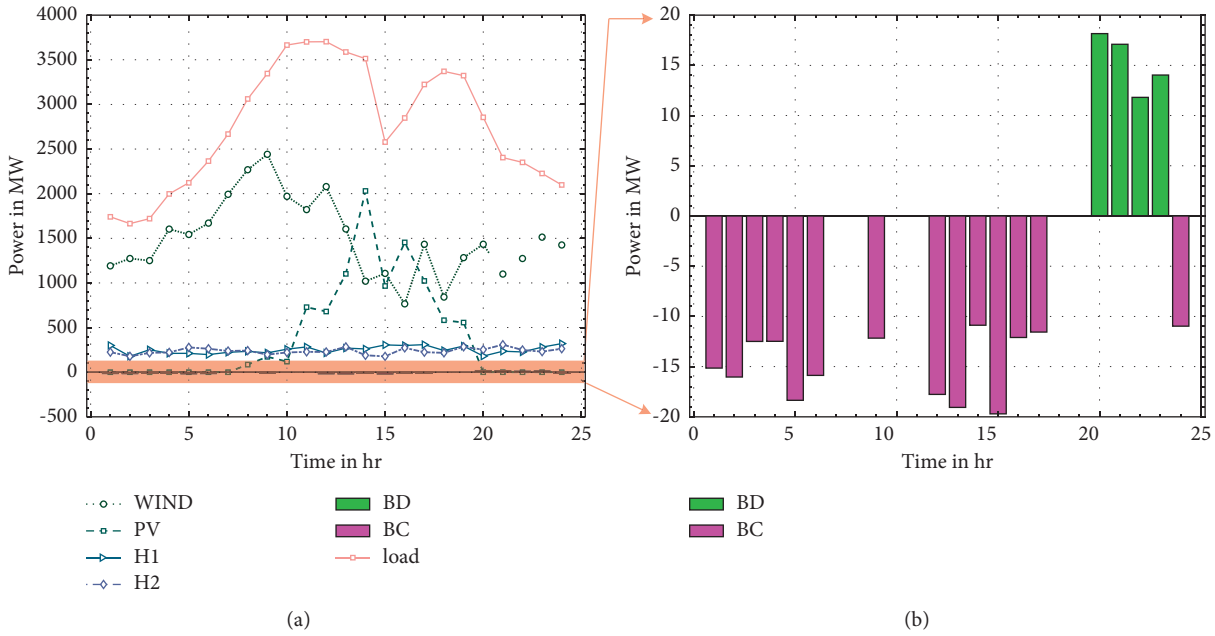

Figure 7: Simulation results of Case 1: (a) Generation unit output results of Case 1. (b) Battery output results of Case 1.

power generation is shown in Figure 5. The RMSE is adopted to measure the accuracy of scenery prediction. The expression of RMSE is as follows:

$$RMES = \sqrt{\frac{1}{m}\sum_{i=1}^{m}\left(x_{o,i} - x_{r,i}\right)^2}, \tag{37}$$

where $x_{o,i}$ is the observed value, $x_{r,i}$ is the true value, and m is the number of observations.

In Figures 4 and 5, 'Observed' is the real observation of the data to be predicted, 'Forecast' is the predicted result. The RMSE of wind power forecast is 190.6511 MW, and the RMSE of PV power generation forecast is 313.0239 MW. By observing the 'Observed' and 'Forecast' curves in Figures 4 and 5, it is found that the 'Forecast' curve can well reflect the power size and trend of the 'Observed' curve. And the RMSE is also small, so the LSTM neural network has good prediction results.

4.2. Scenario Generation and Reduction of Wind Power and PV. The instability and randomness of clean energy have negative effects on the safe and stable operation of power systems with access to clean energy, thus it is necessary to discuss the uncertainty of clean energy. In this paper, the LHS method is used to generate 1000 scenery scenarios to describe their uncertainty. To reduce the calculation pressure, the synchronous back reduction algorithm is used to reduce the scenery scenarios, and 10 representative scenarios are generated for economic scheduling research. 1000 wind power and 1000 PV power generation scenarios generated by LHS are shown in Figure 6(a) and Figure 6(b), respectively. The 10 typical wind power and PV power generation scenarios generated by synchronous back generation reduction algorithm are shown in Figure 6(c) and Figure 6(d), respectively, in which s1, s2 ... s10 represent 10 scenarios.

The LHS data of wind power is the first 24 points in Figure 4, and the PV LHS data is the 25th to 48th points in Figure 6. 1000 samples are taken for measuring the prediction errors of wind power and PV, respectively, and 1000 groups of sampling data are superimposed on the prediction curve to obtain 1000 wind power output scenarios as shown in Figure 6(a) and Figure 6(b). To reduce the pressure of calculation, the 10 typical wind and PV output scenarios generated by the synchronous back reduction method are shown in Figure 6(c) and Figure 6(d). The 10 typical scenarios generated can well represent 1000 scenarios of wind power and PV power generation from the output range and output direction.

4.3. Influence of CSP Power Station on Wind Power and PV. The output results of each generation unit in Case 1 are shown in Figure 7(a), and the charge and discharge of the battery are shown in Figure 7(b). The results of Case 2 are shown in Figure 8(a); Figure 8(b) is the output of the storage battery and CSP power station. In the simulation picture, 'WIND' represents wind power, 'PV' is photovoltaic, 'H1' and 'H2' mean two hydropower stations, 'BD' and 'BC' represent battery discharge and charging, respectively, 'CSPD' and 'CSPC' are CSP power station discharge and charging, respectively, and 'load' represents the load of the system. If 'BD' and 'CSPD' are positive, it means that the battery and CSP power station are discharging, and 'BC' and 'CSPC' are negative, it means that the battery and CSP power station are charging. The abscissa is time and the ordinate is output power.

To reflect the influence of CSP power stations on the output of wind power and PV, the fluctuation rate of wind

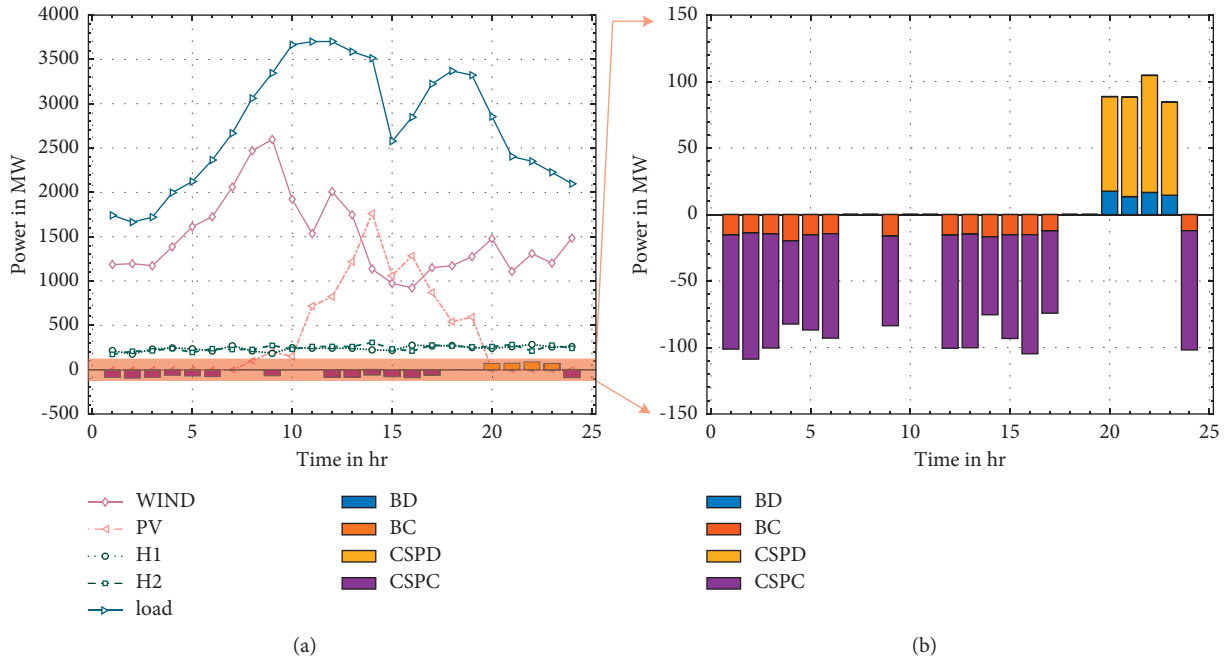

Figure 8: Simulation results of Case 2: (a) Generation unit output results of Case 2. (b) Battery and CSP power station output results of Case 2.

Table 4: Fluctuation rate of wind power and PV of three cases.

Case	1	2	3
Wind volatility	0.998	0.6178	0.6241
PV volatility	6.4348	4.8748	4.7650
Wind and PV volatility	7.4328	5.4926	5.3891

Table 5: Curtailment rate of wind power and PV of three cases.

Case	1	2	3
Wind and PV curtailment	0.3625	0.3576	0.3539

power and PV and the curtailment rate of wind power and PV are defined. The specific expression is as follows:

(1) The fluctuation rate of wind power and PV:

$$\gamma_t = \frac{(P_t - P_{t-1})}{P_{t-1}}, \tag{38}$$

where P_t, P_{t-1} is the output power of wind power and PV in t and $t-1$, γ_t is the fluctuation rate of wind power and PV.

(2) The curtailment rate of wind power and PV:

$$\alpha = \frac{(\mathrm{PV}_0 + \mathrm{WIND}_0 - \mathrm{PV}_1 - \mathrm{WIND}_1)}{(\mathrm{PV}_0 + \mathrm{WIND}_0)}, \tag{39}$$

where PV_0 and $WIND_0$ are the output power of PV station and wind power station, PV_1 and $WIND_1$ are the actually used PV and wind power in an economic dispatch, α is the curtailment rate of wind power and PV.

To verify the effect of CSP power stations on system regulation performance, the wind power and PV output curves in Figure 7(a) and Figure 8(a) are compared. It can be found that the wind power and PV output curves in Figure 8(a) are relatively stable compared with those in

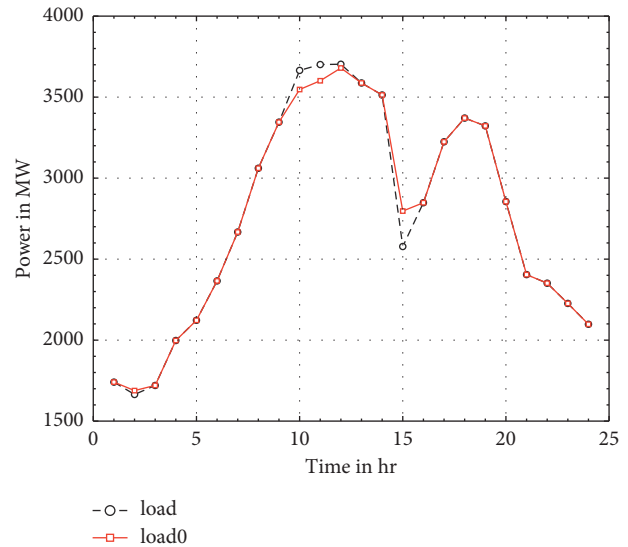

Figure 9: Load before translation and load after translation.

Figure 7(a). Most obviously the load curve fluctuates greatly from 14 : 00 to 15 : 00, specifically, the PV output changes by 1066 MW from 14 : 00 to 15 : 00 in Case1, and by 703 MW in Case 2, which is due to the addition of CSP power station in Case 2. The output of the hydropower station is increased in Case 2 from 14 : 00 to 15 : 00, and stored the excess PV

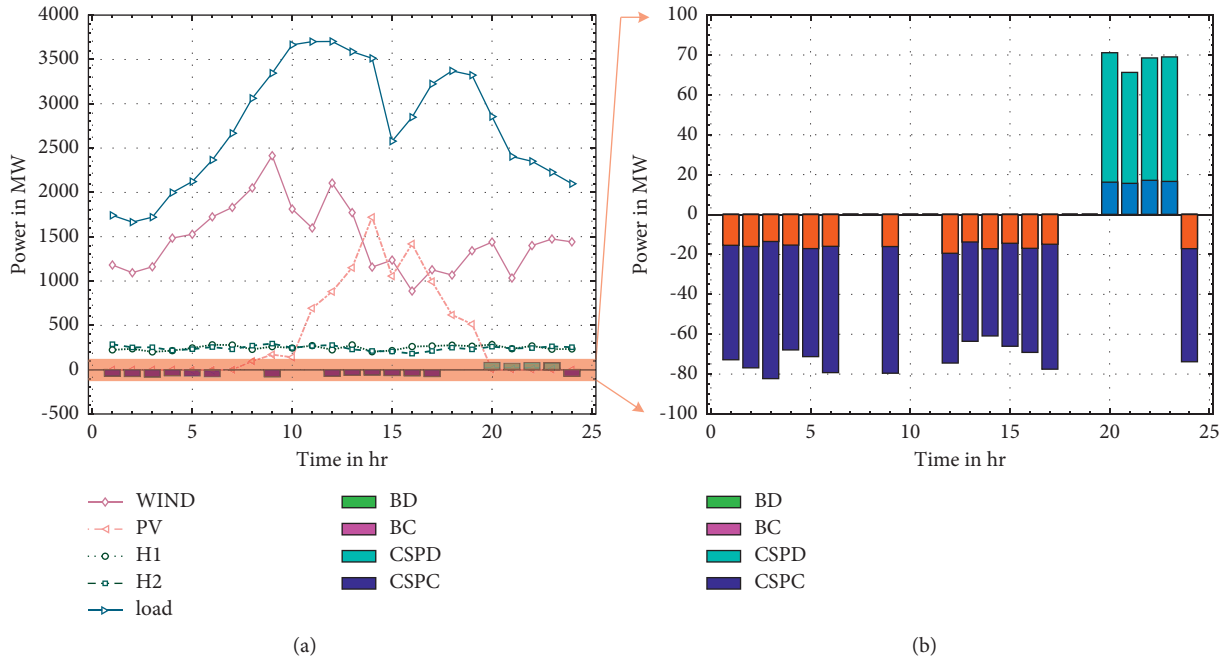

Figure 10: Simulation results of Case 3: (a) Generation unit output results of Case 3. (b) Battery and CSP power station output results of Case 3.

output in CSP power station and storage battery, making the PV output curve relatively stable. At the same time, it can be found from Table 4 that the fluctuation rate of wind power and PV is 5.4926 in Case 2, which is smaller than that of Case 1, which is 7.4328.

It can be seen from Figure 7(b) and Figure 8(b) that after adding CSP power station, excess wind power and PV are stored in CSP power station and battery at 1 : 00–6:00 and 12 : 00–17 : 00 with sufficient wind and PV output. At 20 : 00–23 : 00 with smaller wind and solar output, CSP power station and battery provide more output to make up for the lack of wind and solar output. At the same time, it can be found in Table 5 that adding CSP power station reduces the curtailment rate of wind power and PV.

4.4. Influence of Transferable Load on Wind Power and PV. To verify the influence of transferable load on system operation, transferable load is considered in Case 3. The fluctuation rate of wind power and PV, and economic cost in three cases are compared. The translatable intervals of translatable load are 9 : 00–10 : 00, 10 : 00–11 : 00, 11 : 00–12 : 00, and the acceptable intervals of translatable load are 1 : 00–2:00, 15 : 00–16 : 00. Figure 9 shows the load curve after translation, in which 'load0' is the load curve before translation and 'load' is the load curve after translation.

The load curve is the load curve after taking the translational load in Case 3. The output curve of each generation unit is shown in Figure 10(a), and the output of CSP power station and the battery is shown in Figure 10(b).

We can see from Figure 10 that after considering the transferable load, the peak-to-valley difference of the system load is reduced, which reduces the flexibility requirements for the output of each unit in the system. At the same time, it can be found from Table 5 that the fluctuation rates of the wind power and PV decrease after the introduction of the translatable load, which is 5.3891, and which is the lowest among the three cases, but its curtailment rates of wind power and PV rates are not much different from those in Case 2. Also, we can see from Table 6 that the economic cost of 4513 $ in Case 3 is higher than that of 4444 $ in Case 2, which is due to the introduction of transferable load compensation cost, but the economic cost is lower than that of Case 1.

Table 6: Economic cost of three cases.

Case	1	2	3
COST/($)	4565	4444	4513

In conclusion, the curtailment rate of wind power and PV rate and the fluctuation rate of wind and PV in Case 2 considering CSP power station are better than those of Case 1 without CSP power station. The fluctuation rate of wind power and PV of Case 3 considering CSP power station and transferable load is better than that of Case 2 considering only CSP power station and Case1 not considering CSP power station and translational load, its curtailment rate of wind power and PV is also better than that of Case 1.

5. Conclusion

In this paper, taking the carbon peak and carbon neutrality as the background, we investigated the economic dispatch of power systems with wind and PV generation as main power supplies. To improve the permeability of wind power and PV power generation and reduce the output uncertainty, this paper established an economic dispatching model including

wind-PV-hydro-CSP-battery and transferable load. The model took the economic cost of the system as the objective function and considered the relevant constraints of wind, PV, hydropower station, CSP power plants, batteries, and transferable load. The following conclusions are obtained:

(1) The wind and PV power generation predicted by LSTM neural network can well reflect their power output, and the RMSE is small in which wind power forecast is 190.6511 MW, PV power generation forecast is 313.0239 MW.

(2) Compared with the traditional renewable energy system with wind power and photovoltaic as energy source, the proposed wind-PV-hydro-CSP-battery system considering transferable load reduces the fluctuation rate of wind and PV power by 27.5%, the reduction of wind and photovoltaic power generation curtailment rate by 2.6% and the economic cost by 1.1%, which prove the effectiveness of the combination of hydropower, CSP power station, battery and transferable load resources in reducing the fluctuation of wind and PV power generation.

In this paper, we find that only considering the flexible resource of transferable load has little impact on reducing the fluctuation of wind and PV power generation. Therefore, we will consider more demand-side response policies in future research.

Nomenclature

C: Total cost
Cg: Cost of the thermal power unit
Cw: Wind power generation cost
C_{pv}: PV power generation cost
C_{csp}: CSP power station cost
C_h: Hydropower generation cost
C_b: Battery cost
C_{tl}: Compensation cost of the transferable load
j: Wind farms index
Nw: Total number of wind farm
$K_{w,j}$: Cost coefficient of the j-th wind farm5
$P_{j,t}$: Output power of the j-th wind farm at time
k: PV power station index
N_{pv}: Total number of PV power station
l: CSP power station index
N_{csp}: Total number of CSP power stations
$K_{CSP,l}$: Operation cost of the l-th CSP power station
$P_{l,t}$: Output power of the l-th CSP power station at time t
$K_{CSP,R,l}$: Spinning reverse cost of the l-th CSP power station
$P_{l,t,r}$: Spinning reverse power of the l-th CSP power station at time t
m: Hydropower station index
N_h: Total number of hydropower stations
N_b: Total number of batteries
$K_{H,m}$: Cost coefficient of the m-th hydropower station
$K_{B,n}$: Cost coefficient of the n-th battery
$P_{m,t}$: Output power of the m-th hydropower station at time
$tts\ tl$: Start time of transferable period
T_{tl}: Original operation time set of transferable load
$C_{tl,t}$: Compensation cost of transferable load at time t
$P_{L,t}$: Load of power system considering the transferable load
$P_{L0,t}$: Load of power system not considering the transferable load
$P_{j,t,f}$: Forecast power of the j-th wind farm at time t
$c_{n,t}$: States of charge of the n-th battery at time t
$P_{n,t}$: Output power of the n-th battery at time t
P_{tl}: Transfer power of the transferable load
$P_{t,tl}$: Power transferred from time t to tl
U_{tl}: Status of the transferable load
$Pmax\ j$: Maximum power of the j-th wind farm
Δt_n: Unit time interval
$P_{j,t,e}$: Forecast error power of the j-th wind farm at time t
$Pmax\ k$: Maximum power of the k-th PV power station
$P_{k,t,f}$: Forecast power of the k-th PV power station at time t
$P_{k,t,e}$: Forecast error power of the k-th PV power station at time t
$Pmax\ l$: Maximum power of the l-th CSP power station
$PTES\ l,t,d$: TES discharge power of the l-th CSP power station at time t
$PTES\ l,t,c$: TES charge power of the l-th CSP power station at time t
$PTES\ l,t,r+$: Positive spinning reserve provided by TES of the l-th CSP power station at time t
$PTES\ l,t,r-$: Negative spinning reserve provided by TES of the l-th CSP power station at time t
$PTES,max\ l,t,d$: TES maximum discharge power of the l-th CSP power station at time t
$PTES,max\ l,t,c$: TES maximum charge power of the l-th CSP power station at time t
RU_{pv}: Up spinning reserve of the power system
RD_s: Down spinning reserve of the power system
$\eta c\ n$: Charge efficiencies
$\eta d\ n$: Discharge efficiencies
$d_{n,t}$: States of discharge of the n-th battery at time t
$te\ tl$: End time of transferable period
$W_{h,f}$: Recursive weight matrixes of f_t
$W_{h,i}$: Recursive weight matrixes of i_t
$W_{h,o}$: Recursive weight matrixes of o_t
$W_{x,f}$: Input weight matrixes of f_t
$W_{x,i}$: Input weight matrixes of i_t
$W_{x,o}$: Input weight matrixes of o_t
b_f: Offset matrixes of f_t
b_i: Offset matrixes of i_t
b_o: Offset matrixes of o_t
μ_t: The mean
σ_t: The variance
v_t: Free degree
$K_{pv,k}$: Cost coefficient of the k-th PV power station
$P_{k,t}$: Output power of the k-th PV power station at time t

$Y_{l,t}$: State variable
Pmax m: Maximum output power of the *m*-th hydropower station
Pmin m: Minimum output power of the *m*-th hydropower station
$V_{m,t}$: Storage capacity of the reservoir of the *m*-th hydropower station at time *t*
$V_{m,t+1}$: Storage capacity of the reservoir of the m-th hydropower station at time *t+1*
Vmax m: Maximum storage capacity of the reservoir of the *m*-th hydropower station
Vmin m: Minimum storage capacity of the reservoir of the *m*-th hydropower station
$Q_{m,t}$: Outflow of the *m*-th hydropower station at time *t*
Qmax m: Maximum outflow of the *m*-th hydropower station
Qmin m: Minimum outflow of the *m*-th hydropower station
$I_{m,t}$: Inflow of the *m*-th hydropower station at time *t*
o: Upstream hydropower station of the *m*-th hydropower station
τ_{om} : Time delay from the *o*-th hydropower station to the *m*-th hydropower station
$Q_{o,(t-\tau om)}$: Outflow of the *o*-th hydropower station by time $(t-\tau om)$
$E_{n,t}$: Capacities of the *n*-th battery at time *t*
$E_{n,t-1}$: Capacities of the *n*-th battery at time *t-1*
Emax n: Maximum capacities of the *n*-th battery
Emin n: Minimum capacities of the *n*-th battery
Pc n,t: Charge power of the *n*-th battery at time *t*
Pd n,t: Discharge power of the *n*-th battery at time *t*
Pc,max n: Maximum charge power of the *n*-th battery
Pd,max n: Maximum discharge power of the *n*-th battery.

Abbreviations

PV: Photovoltaic
CSP: Concentrating solar power
LSTM: Long short-term memory
CFCEP: Chaotic fast convergence evolutionary programming
LHS: Latin hypercube sampling
GA: Genetic algorithm
SQP: Sequential quadratic programming
AGC: Automatic generation control
TES: Thermal energy storage
RNN: Recurrent neural network
RMSE: Root means square error.

Data Availability

Detailed data can be found within the article.

Conflicts of Interest

The authors declare that they have no conflicts of interest.

Acknowledgments

This work was supported in part by the National Natural Science Foundation of China under Grant no U2003110 and in part by the Key Laboratory Project of Shaanxi Provincial Department of Education (No. : 20JS110) and Shaanxi Youth Science and Technology New Star Project (No. : 2020KJXX-094) and Xi'an Science and Technology Planning Project (No. : 2020KJRC0084).

References

[1] H. Anna, A. Caitlin, J. C. Wesley, and L. D. Paul, "The evolving energy and capacity values of utility-scale PV-plus-battery hybrid system architectures," *Advances in Applied Energy*, vol. 2, no. 26, Article ID 100015, 2021.

[2] R. Sadiq, Z. Wang, C. Y. Chung, C. Zhou, and C. Wang, "A review of STATCOM control for stability enhancement of power systems with wind/PV penetration: Existing research and future scope," *International Transactions on Electrical Energy Systems*, vol. 31, 2021.

[3] Z. C. Deng, J. Y. Xiao, S. K. Zhang, Y. Xie, Y. Rong, and Y. Zhou, "Economic feasibility of large-scale hydro-solar hybrid power including long distance transmission," *Global Energy Interconnection*, vol. 2, no. 4, pp. 290–299, 2019.

[4] J. Z. Yang, Z. Yang, and Y. Y. Duan, "Optimal capacity and operation strategy of a solar-wind hybrid renewable energy system," *Energy Conversion and Management*, vol. 244, no. 15, Article ID 114519, 2021.

[5] N. Varghese and P. Reji, "Energy storage management of hybrid solar/wind standalone system using adaptive neuro-fuzzy inference system," *International Transactions on Electrical Energy Systems*, vol. 29, no. 7, Article ID e12124, 2019.

[6] S. Angadi, U. R. Yaragatti, Y. Suresh, and A. B Raju, "An effective standalone hybrid wind-photovoltaic water pumping system with reduced power converter count," *International Transactions on Electrical Energy Systems*, vol. 31, no. 12, Article ID e13140, 2021.

[7] T. G. Hlalele, R. M. Naidoo, R. C. Bansal, and J. Zhang, "Multi-objective stochastic economic dispatch with maximal renewable penetration under renewable obligation," *Applied Energy*, vol. 270, Article ID 115120, 2020.

[8] Y. Yin, T. Q. Liu, and C. He, "Day-ahead stochastic coordinated scheduling for thermal-hydro-wind -photovoltaic systems," *Energy*, vol. 187, no. 0360-5422, Article ID 115944, 2019.

[9] M. Basu, "Multi-region dynamic economic dispatch of solar–wind–hydro–thermal power system incorporating pumped hydro energy storage," *Engineering Applications of Artificial Intelligence*, vol. 86, no. 0952-1976, pp. 182–196, 2019.

[10] F. Merahi, A. E. Badoud, and S. Mekhilef, "A novel power management strategies in PV-wind-based grid connected hybrid renewable energy system using proportional distribution algorithm," *International Transactions on Electrical Energy Systems*, vol. 31, no. 7, Article ID e12931, 2021.

[11] Y. W. Zhang, J. Yang, X. L. Pan et al., "Data-driven robust dispatch for integrated electric-gas system considering the correlativity of wind-solar output," *International Journal of Electrical Power & Energy Systems*, vol. 134, Article ID 107454, 2022.

[12] Q. L. Tan, S. F. Mei, M. Dai, L. Zhou, Y. Wei, and L. Ju, "A multi-objective optimization dispatching and adaptability analysis model for wind-PV-thermal-coordinated operations considering comprehensive forecasting error distribution," *Journal of Cleaner Production*, vol. 256, Article ID 120407, 2020.

[13] Y. W. Zhang, J. X. Xiao, and J. Yang, "Data-driven robust economic dispatch for distribution network and multiple micro-grids considering correlativity of wind and solar output," *Electric Power Construction*, vol. 42, no. 10, pp. 40–50, 2021.

[14] F. T. Hu, K. J. Hughes, D. B. Ingham, L. Ma, and M. Pourkashanian, "Dynamic economic and emission dispatch model considering wind power under energy market reform: a case study," *International Journal of Electrical Power & Energy Systems*, vol. 110, no. 0142-0615, pp. 184–196, 2019.

[15] D. Ershun, N. Zhang, B. S. Hodge, C. Kang, K. Benjamin, and X. Qing, "Economic justification of concentrating solar power in high renewable energy penetrated power systems," *Applied Energy*, vol. 222, no. 0306-2619, pp. 649–661, 2018.

[16] D. Ershun, N. Zhang, B. S. Hodge, C. Kang, K. Benjamin, and X. Qing, "The role of concentrating solar power toward high renewable energy penetrated power systems," *IEEE Transactions on Power Systems*, vol. 33, no. 6, pp. 6630–6641, 2018.

[17] J. W. Bai, T. Ding, Z. Wang, and W. Chen, "Day-ahead robust economic dispatch considering renewable energy and concentrated solar power plants," *Energies*, vol. 12, no. 20, p. 3832, 2019.

[18] M. Basu, "Economic environmental dispatch of solar-wind-hydro-thermal power system," *Renewable Energy Focus*, vol. 30, no. 1755-0086, pp. 107–122, 2019.

[19] H. Yu, J. H. Zhang, K. Wong, C. Y. Chung, and H. Lee, "Probabilistic load flow evaluation with hybrid Latin hypercube sampling and cholesky decomposition," *IEEE Transactions on Power Systems*, vol. 24, no. 2, pp. 661–667, 2009.

[20] W. X. Wang, C. S. Li, X. Liao, and H. Qin, "Study on unit commitment problem considering pumped storage and renewable energy via a novel binary artificial sheep algorithm," *Applied Energy*, vol. 187, pp. 612–626, 2017.

[21] A. Merabet, K. Tawfique Ahmed, H. Ibrahim, R. Beguenane, and A. M. Y. M. Ghias, "Energy management and control system for laboratory scale microgrid based wind-PV-battery," *IEEE Transactions on Sustainable Energy*, vol. 8, no. 1, pp. 145–154, 2017.

[22] X. Q. Xu, Y. Chen, Y. Goude, and Q. Yao, "Day-ahead probabilistic forecasting for French half-hourly electricity loads and quantiles for curve-to-curve regression," *Applied Energy*, vol. 301, no. 1, Article ID 117465, 2021.

[23] J. Q. Tian, Y. J. Wang, and Z. H. Chen, "Sensor fault diagnosis for lithium-ion battery packs based on thermal and electrical models," *International Journal of Electrical Power & Energy Systems*, vol. 121, Article ID 106087, 2020.

[24] Q. L. Tan, S. F. Mei, Q. Ye, Y. Ding, and Y. Zhang, "Optimization model of a combined wind–PV–thermal dispatching system under carbon emissions trading in China," *Journal of Cleaner Production*, vol. 225, pp. 391–404, 2019.

[25] H. Ghoddami, M. B. Delghavi, and A. Yazdani, "An integrated wind-photovoltaic-battery system with reduced power-electronic interface and fast control for grid-tied and off-grid applications," *Renewable Energy*, vol. 45, pp. 128–137, 2012.

[26] C. M. Lai and J. Teh, "Network topology optimisation based on dynamic thermal rating and battery storage systems for improved wind penetration and reliability," *Applied Energy*, vol. 305, Article ID 117837, 2022.

[27] U. Datta, A. Kalam, and J. Shi, "The relevance of large-scale battery energy storage (BES) application in providing primary frequency control with increased wind energy penetration," *Journal of Energy Storage*, vol. 23, pp. 9–18, 2019.

[28] E. Pusceddu, B. Zakeri, and G. Castagneto Gissey, "Synergies between energy arbitrage and fast frequency response for battery energy storage systems," *Applied Energy*, vol. 283, Article ID 116274, 2021.

[29] X. Q. Ren, S. L. Liu, X. D. Yu, and X. Dong, "A method for state-of-charge estimation of lithium-ion batteries based on PSO-LSTM," *Energy*, vol. 234, no. 1, Article ID 121236, 2021.

[30] B. C. Li, H. J. Yu, and J. Y. Liu, "Prediction of short-term PV power generation based on kmeans and CEEMD-PE-LSTM [J]," *Water Resources and Power*, vol. 39, no. 4, pp. 204–208, 2021.

[31] S. R. Ara, S. Paul, and Z. H. Rather, "Two-level planning approach to analyze techno-economic feasibility of hybrid offshore wind-solar pv power plants," *Sustainable Energy Technologies and Assessments*, vol. 47, Article ID 101509, 2021.

[32] M. Fasihi, R. Weiss, J. Savolainen, and C. Breyer, "Global potential of green ammonia based on hybrid PV-wind power plants," *Applied Energy*, vol. 294, no. 15, Article ID 116170, 2021.

[33] J. Q. Tian, R. L. Xu, Y. J. Wang, and Z. Chen, "Capacity attenuation mechanism modeling and health assessment of lithium-ion batteries," *Energy*, vol. 221, Article ID 119682, 2021.

[34] Z. F. Tan, W. Fan, H. F. Li et al., "Dispatching optimization model of gas-electricity virtual power plant considering uncertainty based on robust stochastic optimization theory," *Journal of Cleaner Production*, vol. 247, Article ID 119106, 2020.

[35] J. Z. Yang, Z. Yang, and Y. Y. Duan, "Load matching and techno-economic analysis of CSP plant with S-CO_2 brayton cycle in CSP-PV-wind hybrid system," *Energy*, vol. 223, no. 15, Article ID 120016, 2021.

[36] O. D. Montoya and W. Gil-González, "Dynamic active and reactive power compensation in distribution networks with batteries: a day-ahead economic dispatch approach," *Computers & Electrical Engineering*, vol. 85, Article ID 106710, 2020.

[37] D. M. Zhao, H. X. Wang, and R. Tao, "Multi-time scale dispatch approach for an AC/DC hybrid distribution system considering the response uncertainty of flexible loads," *Electric Power Systems Research*, vol. 199, Article ID 107394, 2021.

[38] A. AbuElrub, H. M. K. Al-Masri, and C. Singh, "Hybrid wind-solar grid-connected system planning using scenario aggregation method," *International Transactions on Electrical Energy Systems*, vol. 30, no. 9, Article ID e12519, 2020.

[39] S. W. Yu, S. S. Zhou, and J. P. Qin, "Layout optimization of China's power transmission lines for renewable power integration considering flexible resources and grid stability," *International Journal of Electrical Power & Energy Systems*, vol. 135, Article ID 107507, 2022.

[40] J. J. Zhang, H. H. Li, D. Y. Chen, B. Xu, and M. A. Mahmud, "Flexibility assessment of a hybrid power system: hydro-electric units in balancing the injection of wind power," *Renewable Energy*, vol. 171, pp. 1313–1326, 2021.